Journal of Solid State Chemistry 184 (2011) 3172–3178

Contents lists available at SciVerse ScienceDirect

Journal of Solid State Chemistry

journal homepage: www.elsevier.com/locate/jssc

A series of 2D lanthanide (III) coordination polymers constructed from 2-(pyridin-3-yl)-1H-imidazole-4,5-dicarboxylate

Song Liang Cai, Sheng Run Zheng*, Jun Fan, Jing Bo Tan, Tian Tian Xiao, Wei-Guang Zhang*

Institute of Special Materials & School of Chemistry and Environment, South China Normal University, Guangzhou 510006, PR China

ARTICLE INFO

Article history:
Received 24 June 2011
Received in revised form
9 September 2011
Accepted 11 September 2011
Available online 22 September 2011

Keywords:
Lanthanide coordination polymers
2-(pyridine-3-yl)-1H-4,5-imidazoledicarboxylic
Lanthanide contraction effect
Photoluminescence

ABSTRACT

Reactions of 2-(pyridine-3-yl)-1H-4,5-imidazoledicarboxylic acid (H_3PyIDC) with a series of *Ln*(III) ions affords ten coordination polymers, namely, $\{[Ln(H_2PyIDC)(HPyIDC)(H_2O)_2]\cdot H_2O\}_n$ [*Ln*=Nd (**1**), Sm (**2**), Eu (**3**) and Gd (**4**)], $\{[Ln(HPyIDC)(H_2O)_3]\cdot(H_2PyIDC)\cdot H_2O\}_n$ [*Ln*=Gd (**5**), Tb (**6**), Dy (**7**), Ho (**8**) and Er (**9**)], and $\{[Y_2(HPyIDC)_2(H_2O)_5]\cdot(bpy)\cdot(NO_3)_2\cdot 3H_2O\}_n$ (**10**) (bpy=4,4′-bipyridine). They exhibit three types of networks: complexes **1**–**4** are isomorphous coordination networks containing neutral 2D metal-organic layers, while complexes **5**–**9** are isomorphous, which consist of cationic metal-organic layers and anionic organic layers, and complex **10** is a 2D network built up from 4-connected $HPyIDC^{2-}$ anion and 4-connected Y(III) ions. In addition, thermogravimetric analyses and solid-state luminescent properties of the selected complexes are investigated. They exhibit intense, characteristic emissions in the visible region at room temperature.

1. Introduction

The construction of coordination polymers has received considerable attention in recent decades, because of their intriguing topologies and their potential applications in catalysis, conductivity, luminescence, magnetism, sensors, nonlinear optics, porosity, etc. [1–5]. Organic ligands containing N and O donors, which can offer versatile coordination modes and potential hydrogen bonding interaction sites, are effective building blocks for constructing various coordination networks [6–9]. Particular attention has been given to the imidazole-4,5-dicarboxylic acid (H_3IDC) ligand, which has a rich coordination chemistry derived from both the imidazole and carboxylic functionalities and can be partially or fully deprotonated to generate H_2IDC^-, $HIDC^{2-}$, and IDC^{3-} anions at different pH values. Therefore, this ligand can coordinate with various metal ions in multi-coordination modes to form a series of metal-organic frameworks (MOFs) with unprecedented topologies and interesting properties [10–18].

These findings on H_3IDC, resulted in increased interest in functionalized H_3IDC ligands with diverse substituent, such as ethyl [19,20], propyl [21], phenyl [22], hydroxymethyl [23], or pyridyl [24–29] groups, at the 2-positon of the imidazole ring. Several research groups have found that the substituent groups may induce a spatial effect on adjacent carboxylate groups. In some case, the substituent groups also provide additional coordination or hydrogen-bonding sites, which further result in the formation of some interesting new MOF materials [19–29].

In the current study, 2-(pyridin-3-yl)-1H- imidazole-4,5-dicarboxylic acid (H_3PyIDC), which is an analog ligands of H_3IDC, was used to assemble new coordination polymers. Published studies on coordination polymers with H_3PyIDC ligand are limited, including only those on $[Mn(H_2PyIDC)_2(H_2O)_2]_n$, $[Fe(H_2PyIDC)_2(H_2O)_2]_n$, and $\{[Nd_3(HPyIDC)_3(PyIDC)]\cdot 2H_2O\}_n$, which have been reported in recent years [26,28,29]. The current study presents the syntheses, structures, and physical properties of 10 new lanthanide coordination polymers assembled from H_3PyIDC exhibiting three kinds of 2D networks. The multiple coordination modes of H_3PyIDC and the lanthanide contraction effect play crucial roles in the network construction of these complexes.

2. Experimental

2.1. Materials and physical measurements

The ligand H_3PyIDC was prepared according to the literature [28]. Lanthanide nitrate hydrates were prepared by dissolving the respective oxides (99.5%) in 1:1 HNO_3 (v/v) followed by drying. All the other reagents were of analytical grade and used without any further purification. Elemental (C, H, N) analyses were preformed on a Thermo FlashEA112 elemental analyzer. IR spectra were recorded by using Perkin–Elmer Spectrum One spectrometer with KBr pellets in the range 4000–400 cm^{-1}. Thermogravimetric analysis (TGA) experiments were carried out

* Corresponding authors. Fax: +86 20 39310187.
E-mail addresses: zhengshengrun@gmail.com (S.R. Zheng), wgzhang@scnu.edu.cn (W.-G. Zhang).

0022-4596/$ - see front matter © 2011 Elsevier Inc. All rights reserved.
doi:10.1016/j.jssc.2011.09.006

on a Netzsch STA409PC Thermal Analyzer with a heating rate of 10 °C/min up to 800 °C under air atmosphere. Solid-state fluorescent spectra were carried out on a Hitachi F-2500 spectrophotometer with a Xenon arc lamp as the light source at room temperature.

2.2. Syntheses of the complexes

2.2.1. Syntheses of $\{[Ln(H_2PyIDC)(HPyIDC)(H_2O)_2]\cdot H_2O\}_n$ [Ln=Nd (**1**), Sm (**2**), Eu (**3**), and Gd (**4**)]

A mixture of $Ln(NO_3)_3\cdot 6H_2O$ (0.10 mmol), H_3PyIDC (23.3 mg, 0.10 mmol), NaOH (2.0 mg, 0.05 mmol), and EtOH/H_2O (1:1, 4 ml) was heated in a 10 ml sample bottle at 105 °C for 48 h. After cooling to room temperature at a rate of 5 °C/h, some crystals suitable for X-ray diffraction analysis were collected manually, washed with water and dried in the air.

Complex **1**, yield: 58%. Calc. for $C_{20}H_{17}N_6NdO_{11}$ (661.64): C, 36.31; H, 2.59; N, 12.70; found: C, 36.42; H, 2.63; N, 12.66%. IR (KBr pellet, cm^{-1}): 3415m, 2924m, 2854w, 2363m, 2343w, 1571s, 1527w, 1449s, 1400s, 1357m, 1330w, 1275m, 1207w, 1119s, 1028w, 976w, 860w, 831w, 804m, 775w, 736w, 702w, 669w, 614m, 535w.

Complex **2**, yield: 62%. Calc. for $C_{20}H_{17}N_6O_{11}Sm$ (667.75): C, 35.97; H, 2.57; N, 12.59; found: C, 36.08; H, 2.61; N, 12.57%. IR (KBr pellet, cm^{-1}): 3413m, 2923w, 2851w, 2361m, 2343w, 1576s, 1529w, 1450s, 1400s, 1359m, 1330w, 1278m, 1190w, 1118s, 1025w, 976w, 860w, 831w, 806m, 775w, 705w, 669w, 614m, 538w.

Complex **3**, yield: 36%. Calc. for $C_{20}H_{17}EuN_6O_{11}$ (669.36): C, 35.89; H, 2.56; N, 12.56; found: C, 35.94; H, 2.55; N, 12.49%. IR (KBr pellet, cm^{-1}): 3416m, 2923s, 2852m, 2366w, 2344w, 1576s, 1451m, 1401s, 1361w, 1260m, 1095w, 1014s, 806s, 775w, 703w, 625w, 611w, 537m, 459w.

Complex **4**, yield: 56%. Calc. for $C_{20}H_{17}GdN_6O_{11}$ (674.65): C, 35.61; H, 2.54; N, 12.46; found: C, 35.24; H, 2.49; N, 12.53%. IR (KBr pellet, cm^{-1}): 3415s, 3228w, 2955w, 2359m, 2341w, 1576s, 1529w, 1500s, 1402s, 1359m, 1278m, 1206w, 1120m, 1027w, 976w, 831w, 809w, 775w, 705w, 669w, 612m, 540w.

Table 1
Crystallographic data and structure refinement summary for **1**–**10**.

Complex Formula	**1** $C_{20}H_{17}NdN_6O_{11}$	**2** $C_{20}H_{17}SmN_6O_{11}$	**3** $C_{20}H_{17}EuN_6O_{11}$	**4** $C_{20}H_{17}GdN_6O_{11}$	**5** $C_{20}H_{19}GdN_6O_{12}$
f_w	661.64	667.75	669.36	674.65	692.66
T (K)	298(2)	298(2)	298(2)	298(2)	298(2)
λ (Å)	0.71073	0.71073	0.71073	0.71073	0.71073
Cryst syst.	Monoclinic	Monoclinic	Monoclinic	Monoclinic	Monoclinic
Space group	P2(1)/c	P2(1)/c	P2(1)/c	P2(1)/c	P2(1)/c
a (Å)	14.588(2)	14.6523(19)	14.6753(13)	14.669(2)	16.0045(18)
b (Å)	13.057(2)	13.0180(17)	13.0120(12)	12.988(2)	11.9723(13)
c (Å)	11.8612(19)	11.8102(15)	11.7854(11)	11.7707(18)	12.9776(14)
α (deg)	90	90	90	90	90
β (deg)	104.100(2)	103.795(2)	103.7210(10)	103.621(2)	111.8070(10)
γ (deg)	90	90	90	90	90
V (Å^3)	2191.1(6)	2187.7(5)	2186.3(3)	2179.5(6)	2308.7(4)
Z	4	4	4	4	4
D_e (g cm^{-3})	2.006	2.027	2.034	2.056	1.993
μ (mm^{-1})	2.449	2.764	2.949	3.123	2.954
F(0 0 0)	1308	1316	1320	1324	1364
GOF on F^2	1.056	1.004	1.025	1.033	1.060
R_1 ($I>2\sigma(I)$)	0.0321	0.0247	0.0219	0.0260	0.0347
wR_2 ($I>2\sigma(I)$)	0.0681	0.0574	0.0516	0.0683	0.0801
R_1 (all data)	0.0436	0.0315	0.0269	0.0289	0.0473
wR_2 (all data)	0.0739	0.0610	0.0544	0.0705	0.0891
Complex Formula	**6** $C_{20}H_{19}TbN_6O_{12}$	**7** $C_{20}H_{19}DyN_6O_{12}$	**8** $C_{20}H_{19}HoN_6O_{12}$	**9** $C_{20}H_{19}ErN_6O_{12}$	**10** $C_{30}H_{34}N_{10}O_{22}Y_2$
f_w	694.33	697.91	700.34	702.67	1064.49
T (K)	298(2)	298(2)	298(2)	298(2)	298(2)
λ (Å)	0.71073	0.71073	0.71073	0.71073	0.71073
Cryst syst.	Monoclinic	Monoclinic	Monoclinic	Monoclinic	Triclinic
Space group	*P*2(1)/*c*	*P*2(1)/*c*	*P*2(1)/*c*	*P*2(1)/*c*	*P*−1
a (Å)	15.9862(12)	15.9560(17)	15.9140(17)	15.9024(16)	11.4107(16)
b (Å)	11.9750(9)	11.9660(13)	11.9588(13)	11.9494(12)	11.6334(16)
c (Å)	12.9496(9)	12.9119(14)	12.8754(14)	12.8469(13)	15.649(2)
α (deg)	90	90	90	90	79.718(2)
β (deg)	111.6240(10)	111.4900(10)	111.3490(10)	111.2340(10)	79.127(2)
γ (deg)	90	90	90	90	73.046(2)
V (Å^3)	2304.5(3)	2293.9(4)	2282.2(4)	2275.5(4)	1934.5(5)
Z	4	4	4	4	2
D_e (g cm^{-3})	2.001	2.021	2.038	2.051	1.827
μ (mm^{-1})	3.150	3.339	3.549	3.771	3.089
F(0 0 0)	1368	1372	1376	1380	1076
GOF on F^2	1.039	1.028	1.081	1.038	1.002
R_1 ($I>2\sigma$(I))	0.0248	0.0219	0.0208	0.0219	0.0506
wR_2 ($I>2\sigma(I)$)	0.0609	0.0500	0.0516	0.0518	0.1023
R_1 (all data)	0.0298	0.0270	0.0242	0.0264	0.0857
wR_2 (all data)	0.0638	0.0525	0.0531	0.0542	0.1186

*2.2.2. Syntheses of $\{[Ln(HPyIDC)(H_2O)_3]\cdot(H_2PyIDC)\cdot H_2O\}_n$ [Ln=Gd (**5**), Tb (**6**), Dy (**7**), ho (**8**), and Er (**9**)]*

A mixture of $Ln(NO_3)_3\cdot 6H_2O$ (0.10 mmol), H_3PyIDC (23.3 mg, 0.10 mmol), 4,4′-bipyridine (bpy, 15.6 mg, 0.10 mmol), NaOH (2.0 mg, 0.05 mmol) and EtOH/H_2O (1:1, 4 ml) was heated in a 10 ml sample bottle at 105 °C for 48 h. After cooling to room temperature at a rate of 5 °C/h, block crystals suitable for X-ray diffraction analysis were collected manually, washed with water and dried in the air.

Complex **5**, yield: 55%. Calc. for $C_{20}H_{19}GdN_6O_{12}$ (692.66): C, 34.68; H, 2.76; N, 12.13; found: C, 34.87; H, 2.69; N, 12.26%. IR (KBr pellet, cm^{-1}): 2923w, 2853w, 2359s, 2341s, 1723w, 1691w, 1580s, 1477m, 1429s, 1400w, 1366m, 1276w, 1233w, 1197w, 1120m, 1027w, 967w, 933w, 863w, 811m, 795w, 723w, 669m, 617w, 599w, 535w.

Complex **6**, yield: 41%. Calc. for $C_{20}H_{19}N_6O_{12}Tb$ (694.33): C, 34.60; H, 2.76; N, 12.10; found: C, 34.48; H, 2.71; N, 12.06%. IR (KBr pellet, cm^{-1}): 2923w, 2858w, 2361w, 2343w, 1578s, 1474m, 1445s, 1398w, 1366s, 1276m, 1231w, 1197w, 1120m, 1027w, 973m, 867w, 813w, 781w, 721m, 702w, 635w, 608w, 538m.

Complex **7**, yield: 63%. Calc. for $C_{20}H_{19}DyN_6O_{12}$ (697.91): C, 34.42; H, 2.74; N, 12.04; found: C, 34.46; H, 2.68; N, 11.98%. IR (KBr pellet, cm^{-1}): 2923w, 2856w, 2359m, 2341w, 1580s, 1474w, 1445s, 1400w, 1366s, 1276m, 1233w, 1197w, 1120s, 1027m, 976m, 863w, 813w, 781w, 720w, 702m, 666w, 626w, 538m.

Complex **8**, yield: 65%. Calc. for $C_{20}H_{19}HoN_6O_{12}$ (700.34): C, 34.30; H, 2.73; N, 12.00; found: C, 34.18; H, 2.65; N, 11.95%. IR (KBr pellet, cm^{-1}): 2923m, 2853w, 2366w, 2343w, 1583s, 1474w, 1431m, 1398w, 1366s, 1276m, 1233w, 1197w, 1120s, 1027w, 976m, 869w, 813w, 781w, 720w, 702w, 614w, 538m.

Complex **9**, yield: 68%. Calc. for $C_{20}H_{19}ErN_6O_{12}$ (702.67): C, 34.19; H, 2.73; N, 11.96; found: C, 34.08; H, 2.78; N, 11.99%. IR (KBr pellet, cm^{-1}): 2923m, 2853w, 2361s, 2343w, 1585s, 1474w, 1447m, 1400w, 1364s, 1262m, 1197w, 1120s, 1027w, 973w, 930w, 863w, 797m, 779w, 723w, 693w, 669m, 635w, 618w, 594w, 542w.

*2.2.3. Synthesis of $\{[Y_2(HPyIDC)_2(H_2O)_5]\cdot(bpy)\cdot(NO_3)_2\cdot 3H_2O\}_n$ (**10**)*

The synthesis of complex **10** was similar to the above description as **5** except that $Gd(NO_3)_3\cdot 6H_2O$ was replaced by $Y(NO_3)_3\cdot 6H_2O$ (38.3 mg, 0.10 mmol). Colorless block crystals of **10** were obtained in a yield of 10%. Calc. for $C_{30}H_{34}N_{10}O_{22}Y_2$ (1064.49): C, 33.85; H, 3.22; N, 13.16; found: C, 33.95; H, 3.19; N, 13.27%. IR (KBr pellet, cm^{-1}): 2953w, 2856w, 2359s, 2341s, 1585s, 1447w, 1366w, 1357w, 1330w, 1262s, 1102s, 1032m, 933w, 908w, 860w, 806s, 721w, 684w, 669m, 655w, 617w, 535w, 506w.

2.3. X-ray Crystallographic analysis

Diffraction data of complexes **1–10** were collected on a Bruker Smart APEX II CCD diffractometer equipped with graphite-monochromated Mo*K*α radiation (λ=0.71073 Å) using the ω-scan technique. Multi-scan absorption corrections were applied with the *SADABS* program [30]. The structures were solved by direct methods using the *SHELXS*-97 program and all the non-hydrogen atoms were refined anisotropically with the full-matrix least-squares on F^2 using the *SHELXL*-97 program [31]. The hydrogen atoms of water molecules and imidazole nitrogens in complexes **1, 3, 6**, and **10** were located in the difference Fourier maps and the other hydrogen atoms were generated geometrically and refined as riding atoms with isotropic thermal factors. Crystallographic data and structure determination summaries for **1–10** are listed in Table 1. The selected bond lengths and angles for **1–10** are listed in Supporting Information, Tables S1 and S2, respectively. CCDC 796100–796109 (**1–10**) contain the supplementary crystallographic data for this paper. Copies of these data can be obtained free of charge from The Cambridge Crystallographic Data Center via www.ccdc.cam.ac.uk/data_request/cif.

3. Results and discussion

3.1. Crystal structure descriptions

*3.1.1. Type **I** structure of complexes **1–4***

X-ray structural analyses reveal that complexes **1–4** are isostructural and have similar structures (type **I**). As a representative example, the crystal structure of **4** is described in detail. Complex **4** crystallizes in the $P2_1/c$ space group, and the asymmetric unit

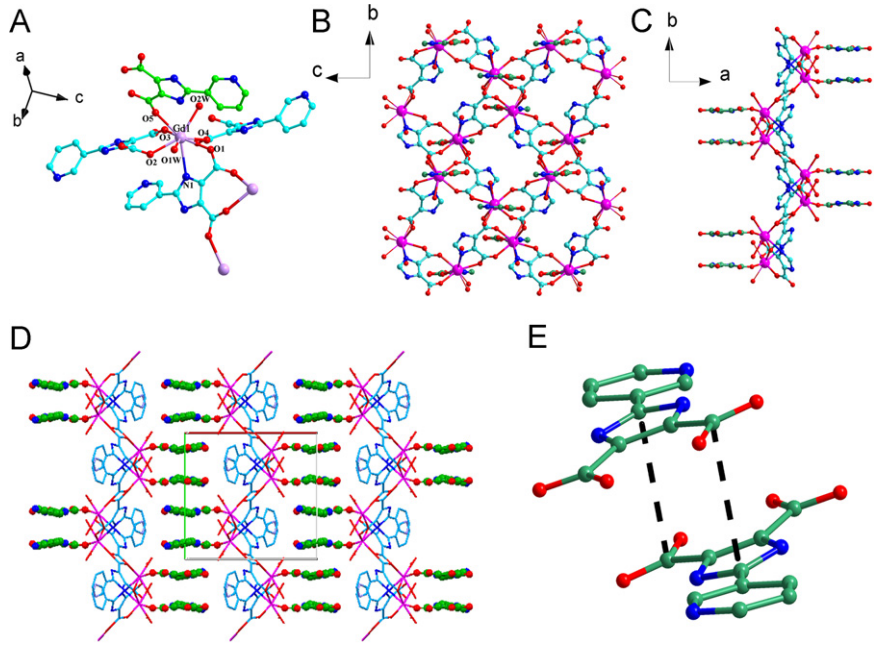

Fig. 1. (A) The coordination environment of Gd(III) in **4**. (B) Top view of the 2D network in **4**. (C) Side view of the 2D network in **4**. (D) The packing of 2D nets along *c* axis in **4**. (E) Lone pair–π interaction between H_2PyIDC^- anions in **4**. The pyridyl groups in (B) and all the H atoms and are omitted for clarity.

contains one Gd(III), one $HPyIDC^{2-}$ anion, one H_2P3IDC^{-} anion, and two coordinated and two uncoordinated water molecules. As shown in Fig. 1A, the Gd(III) ion is eight-coordinated and has a distorted dodecahedral coordination configuration composed of one imidazole nitrogen and four carboxylate oxygen atoms from three different $HPyIDC^{2-}$ moieties, one carboxylate oxygen atom from the H_2PyIDC^{-} moiety, and two terminal water molecules. The Gd–O bond lengths range from 2.317(2) to 2.445(2) Å and the Gd–N bond length is 2.584(3) Å. The Nd–O (**1**), Sm–O (**2**), and Eu–O (**3**) bonds are slightly longer than the corresponding Gd–O bonds in **4** (Table S1) because of the lanthanide contraction effect. In complex **4**, the $HPyIDC^{2-}$ anions adopt μ_3 coordination modes, such as the *N*,*O*-chelating, *O*′,*O*″-chelating, and monodentate O modes (Scheme 1), and connect with the adjacent Gd(III) ions to generate a 2D cationic network. The H_2PyIDC^{-} anion then acts as a monodentate ligand (Scheme 1) to occupy one site in the coordination sphere of the Gd(III) ion, resulting in a neutral 2D coordination layer (Fig. 1B and C). All H_2PyIDC^{-} anions located on the surface are almost perpendicular to this 2D layer. Moreover, the adjacent neutral 2D layers are linked via diverse H-bonds (Table S2) involving $HPyIDC^{2-}$ anions, uncoordinated water molecules, and H_2PyIDC^{-} anions, etc., thereby generating a 3D supramolecular network (Fig. 1D). In addition, the distance between the carboxylate C atom of the H_2PyIDC^{-} anion and the center of the imidazolyl group of another H_2PyIDC^{-} anion is 3.307 Å, indicating a weak lone pair-π interaction (Fig. 1E) [32], which further increases the stability of the 3D supramolecular network.

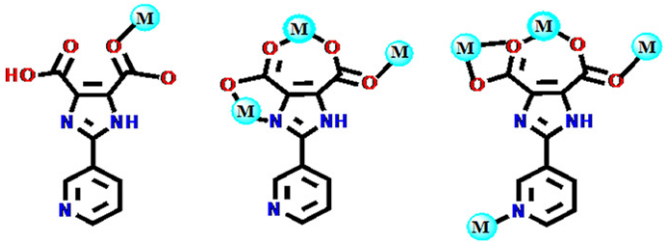

Scheme 1. Coordination modes of H_3PyIDC in complexes **1**–**10**.

3.1.2. *Type **II** structure of complexes **5**–**9***

Complexes **5**–**9** are isostructural and exhibit the type **II** structure, which crystallizes in the $P2_1/c$ space group; only the structure of **5** is described in detail as an example. The asymmetric unit of **5** contains one Gd(III) ion, one $HPyIDC^{2-}$ anion, one free H_2PyIDC^{-} anion, and three ligated and one lattice water molecules. The coordination environment and geometry of Gd(III) in **5** are similar to those of complex **4**, except that the monodentate H_2PyIDC^{-} anion is replaced with a water molecule (Fig. 2A). The Gd–O bond length ranges from 2.322(4) to 2.438(4) Å and Gd–N bond length is 2.546(4) Å, which is slightly shorter compared to that of complex **4**. The Gd–O bonds are slightly longer than the corresponding *Ln*–O bonds in complexes **6–9** (Table S1).

In complex **5**, the μ_3-$HPyIDC^{2-}$ anions link with the adjacent Gd(III) ions to form a 2D cationic coordination layer (Fig. 2B), whereas the uncoordinated H_2PyIDC^{-} anions exist in the lattice and form hydrogen bonds with the coordinated water molecules (Fig. 2C). Thus, this 2D cationic layer is regarded as a separate organic layer (Fig. 2D). In addition, a series of acceptor/donor hydrogen bonds (Table S2) link the 2D layers to form a 3D supramolecular network.

The difference between the type **I** and type **II** structures is the ability of the H_2PyIDC^{-} anions to bind the Gd(III) ions. If the Gd(III) ions and the organic connectors ($HPyIDC^{2-}$) can be regarded topologically as 3-connected nodes, then the overall 2D network in type **I** and type **II** structures can be simplified to a 3-connected $(4\cdot8^2)$ topology (Fig. 2E).

3.1.3. *Type **III** structure of complex **10***

Complex **10** crystallizes in the triclinic space group $P-1$, with the asymmetric unit consisting of two crystallographically independent Y(III) ions, two $HPyIDC^{2-}$ ligands, one bpy molecule, two NO_3^- anions, and five coordinated, and three uncoordinated water molecules. As shown in Fig. 3 A, the Y1 ion is eight-coordinated by five oxygen atoms, one nitrogen atom from four different $HPyIDC^{2-}$ ligands, and two oxygen atoms from two water molecules to give the distorted dodecahedral geometry. The Y2 ion coordinates with five oxygen atoms and one nitrogen atom from four different $HPyIDC^{2-}$ anions and three oxygen atoms

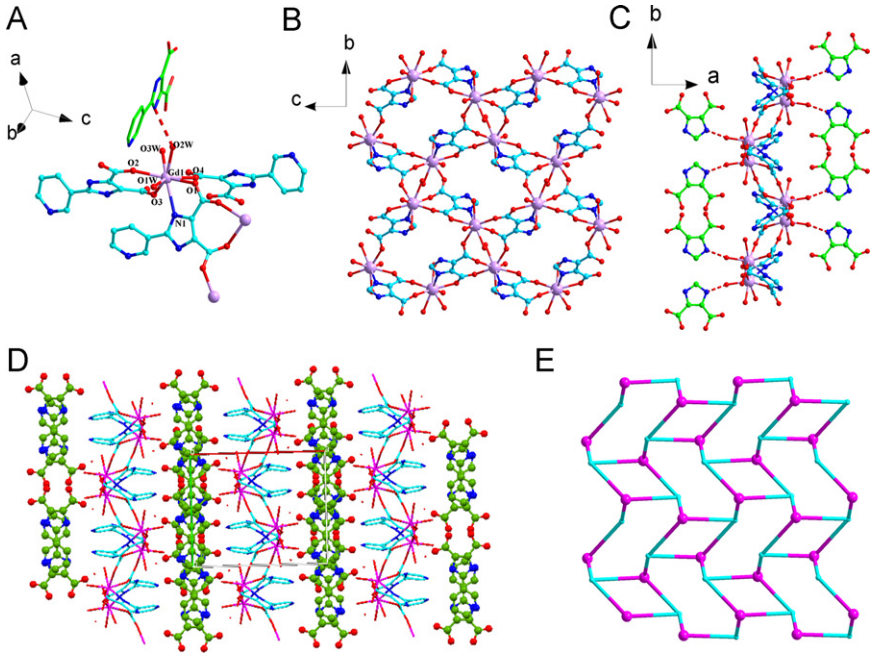

Fig. 2. (A) The coordination environment of Gd(III) in **5**. (B) Top view of the 2D network in **6**. (C) Side view of the 2D network in **5**. (D) The packing of 2D nets along *c* axis in **5**. (E) $(4\cdot8^2)$ topology of the 2D network in **4** and **5**. The pyridyl groups in (B) and all the H atoms and are omitted for clarity.

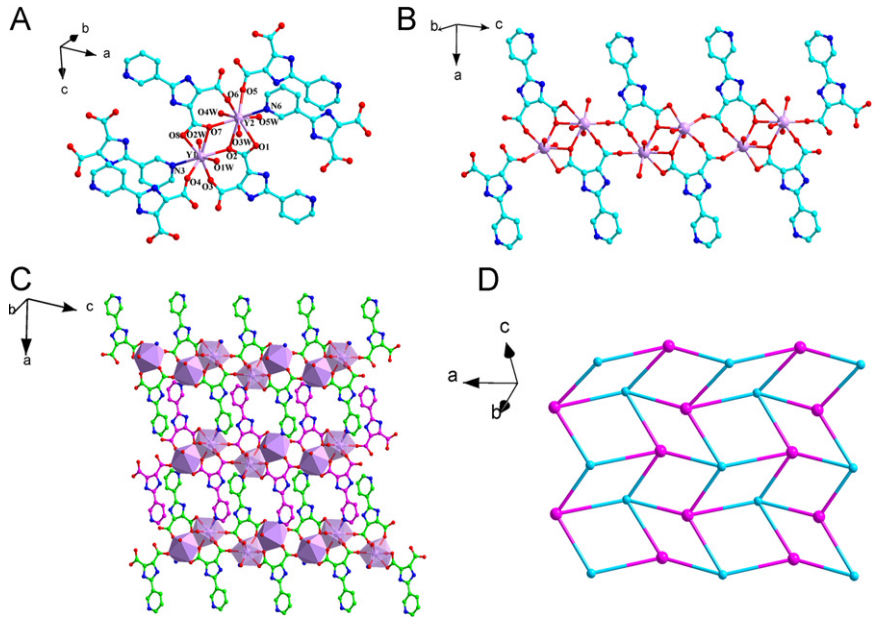

Fig. 3. (A) The coordination environment of Y(III) in **10**. (B) View of 1D zigzag structure of **10**. (C) The 2D sheets constructed by 1D zigzag chain in **10**. (D) Topological view of 2D sheet in **10**. H atoms omitted for clarity.

from three water molecules — nine donor atoms forming a distorted tricapped trigonal prism configuration. The imidazole dicarboxylate motif adopts the μ_3-*k*O, O′: *k*O′, O″: *k*O‴ coordination modes to bridge three Y(III) ions and form a 1D infinite zigzag chain (Fig. 3B). The shortest Y···Y distance is 4.1715(7) Å, whereas the others are 5.4983(8) and 5.8721(8) Å, respectively. Moreover, the pyridyl groups in the $HPyIDC^{2-}$ anions further link the Y(III) ions in the neighboring 1D chains to form a 2D network (Fig. 3C). Therefore, each Y(III) ion coordinating to four $HPyIDC^{2-}$ ligands acts as a 4-connected node and each $HPyIDC^{2-}$ ligand can be regarded as a 4-connected linker, so that a (4,4) network is formed by the connection between the Y(III) centers and the $HPyIDC^{2-}$ anions (Fig. 3D). In addition, these 2D layers are retained by diverse hydrogen bonds involving bpy molecules, NO_3^- anions, and water molecules (Table S2).

3.1.4. Structural comparison of complexes *1–10*

Complexes **6–9** can also be synthesized via the method used to form complexes **1–4** (described above), but with lower yields. Complexes **1–4** can also be synthesized via the method used to generate complexes **6–9** (described above), but also with lower yields.

X-ray diffraction studies reveal that the 10 lanthanide complexes reported in the current study, can be classified into three types based on structure features: neutral 2D layers for **1–4** (type **I**), cationic 2D metal-organic as well as anionic organic layers for **5–9** (type **II**), and a (4,4)-connected 2D network (type **III**). The lanthanide contraction effect clearly played a crucial role in the formation of compounds **1–9**. Although possessing the same coordination number and geometry [33–36], the type **I** and type **II** complexes slightly differ in one of the coordination atoms: one of the coordination sites in complexes **1–4** is occupied by one carboxylate oxygen atom of the monodentate H_2PyIDC^- anion, whereas a ligated water molecule occupies the corresponding site in complexes **5–9**. The combinations between the smaller-radius *Ln*(III) ions and the small donors contributed to the reduced steric hindrance around the metal center compared with the *Ln*(III) ions with bigger radii, and explain the slight difference in the two types of complexes. In addition, the variation in the *Ln*–O bond distances in the series of complexes exhibits the contraction effects. The *Ln*–O bonds in complexes **1–4** are slightly longer than those in complexes **5–9** (Table S1), and the Gd(III) ion is located at a turning point, at which the Gd(III) complexes display two different structural features.

Type **III** structure is quite different from the type **I** and type **II** structures, primarily because of the multiple coordination modes of the H_3PyIDC ligands. In the current study, the H_3PyIDC ligand adopts three kinds of coordination modes (Scheme 1). For complexes **1–9**, the pyridine nitrogen atom remains uncoordinated and the coordination modes of the $HPyIDC^{2-}$ anion are similar to that of H_3IDC. In complex **10**, the pyridine nitrogen atom of the $HPyIDC^{2-}$ ligand is involved in the coordination with the *Ln*(III) ion, which leads to a completely new coordination network.

3.2. XRPD patterns and thermogravimetric analyses

As illustrated in Figs. S1–S10, all the peaks in the measured X-ray powder diffraction patterns of complexes **1–10** closely match those simulated based on the single-crystal structures, suggesting that the crystal samples are pure. The difference in reflection intensity between the simulated and experimental patterns is due to a certain degree of preferred orientation of the powder samples during data collection.

Complexes **4**, **8**, and **10** were taken as the representative examples of the different complexes in the thermogravimetric (TG) analysis to determine their thermal stabilities. Both complexes **4** and **8**, exhibit the similar thermal behaviors as shown in Figs. S21–S22. The first weight loss of 7.0% from 35 to 200 °C in complex **4** corresponds to the removal of all the coordinated and uncoordinated water molecules in the asymmetric unit (calcd 8.1%). The second weight loss in the range from 200 to 500 °C is attributable to the decomposition of the whole coordination network. The TGA curve of complex **8** indicated that the first weight loss of 8.6% in the range of 35–200 °C is ascribed to the elimination of all the water molecules (calcd 9.3%). A major weight loss occurred in the next step, which may correspond to the collapse of the coordination structures. For **10**, the weight loss of 14.1% between 35 and 180 °C may be ascribed to the release of all water molecules per formula unit (calcd 13.5%). The compound does not exhibit weight change up to 300 °C, and the framework starts to collapse at temperatures above 300 °C.

3.3. Luminescent properties

Due to the excellent luminescent properties of the Eu(III) and Tb(III) ions in the visible region, the photoluminescence of **3** and **6** in the solid state was investigated at room temperature.

As shown in Fig. 4, the emission spectrum of complex **3** displays the characteristic *f–f* transition of the Eu(III) ion upon the excitation at 362 nm, implying the ligand-to-europium energy transfer is efficient under the experimental conditions. The emission spectrum is dominated by the characteristic $^5D_0 \rightarrow {}^7F_2$ electron dipole transition at 616 nm. This transition is more intense than the $^5D_0 \rightarrow {}^7F_1$ transition at about 593 nm and the intensity ratio $I(^5D_0 \rightarrow {}^7F_2)/I(^5D_0 \rightarrow {}^7F_1)$ is equal to 2.14, indicating that the Eu(III) ions have a low symmetric coordination environment [37–39], which is in agreement with the result of the X-ray crystal structure analysis of **3**. In addition, two weak peaks at 653 nm and 704 nm can be attributed to the $^5D_0 \rightarrow {}^7F_3$ and $^5D_0 \rightarrow {}^7F_4$ transition, respectively.

Complex **6** emits green light when excited at 330 nm and the emission spectrum exhibits the characteristic transition of $^5D_4 \rightarrow {}^7F_J$ (J=3–6) of the Tb(III) ion with a decay lifetime of 196.0 μs, as shown in Fig. 5. All the transitions to the ground-state manifold from the emitting $^5D_4$ level are observed under the experimental conditions. Two intense emission bands at 489 nm and a sharp line emission at 544 nm correspond to $^5D_4 \rightarrow {}^7F_6$ and $^5D_4 \rightarrow {}^7F_5$ transition, while the weaker emission bands at 584 nm and 621 nm originate from the $^5D_4 \rightarrow {}^7F_4$ and $^5D_4 \rightarrow {}^7F_3$ transition, respectively. The most intense $^5D_4 \rightarrow {}^7F_5$ transition consists of an intense band and one weak shoulder at higher wavelength and the others are less intense broad peaks with small shoulders at lower frequency, which are similar to the reported Tb(III) complexes [40,41].

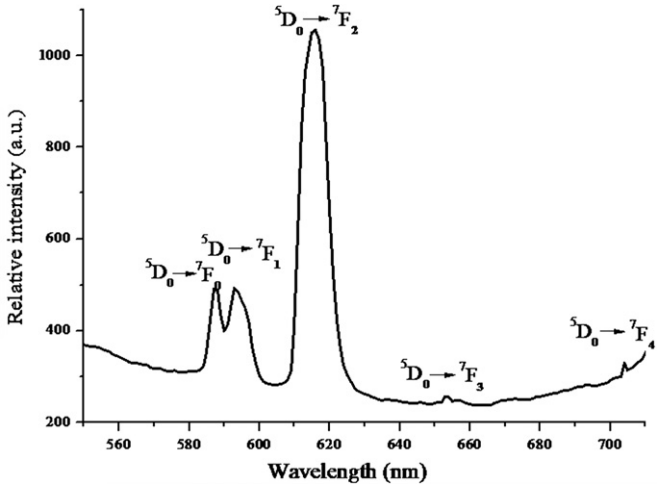

Fig. 4. Solid-state emission spectrum for **3** at room temperature (excited at 362 nm).

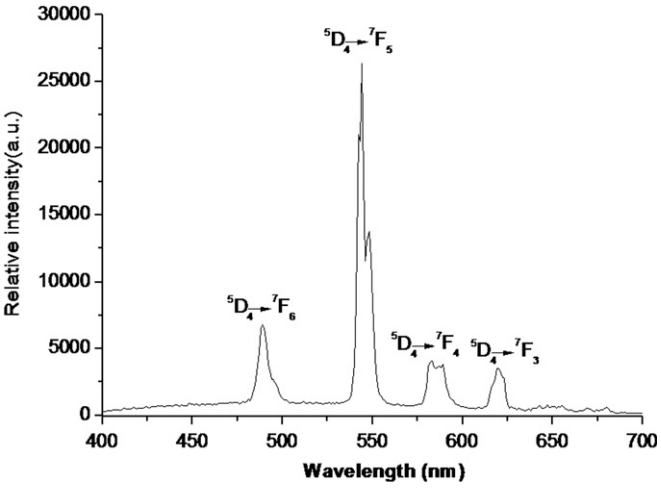

Fig. 5. Solid-state emission spectrum for **6** at room temperature (excited at 330 nm).

4. Conclusion

The multifunctional ligand H_3PyIDC containing both pyridyl and imidazole dicarboxylic motifs was used in the construction of new lanthanide coordination polymers. The resulting complexes **1–10** exhibit diversified 2D structural topologies. The lanthanide contraction effect plays a crucial role in the formation of these complexes. The Gd(III) complex, which is located at a turning point, and its structure can be tuned by using different synthesis strategies. Moreover, H_3PyIDC exhibits diverse coordination modes and is a good candidate for constructing novel frameworks.

Acknowledgment

This work was financially supported by the National Natural Science Foundation of PR China (Grant no. 21003053) and the Ministry of Science and Technology of China (No. 10C26214412704) and the Natural Science Foundation of Guangdong Province (Grant no. 10451063101004667).

Appendix A. Supporting materials

Supplementary data associated with this article can be found in the online version at doi:10.1016/j.jssc.2011.09.006.

References

[1] C.M.G. dos Santos, A.J. Harte, S.J. Quinn, T. Gunnlaugsson, Coord. Chem. Rev. 252 (2008) 2512–2527.
[2] P. Wang, J.P. Ma, Y.B. Dong, R.Q. Huang, J. Am. Chem. Soc. 129 (2007) 10620–10621.
[3] P.K. Thallapally, J. Tian, R.K. Motkuri, C.A. Fernandez, S.J. Dalgarno, P.B. McGrail, J.E. Warren, J.L. Atwood, J. Am. Chem. Soc. 130 (2008) 16842–16843.
[4] M. Shibasaki, N. Yoshikawa, Chem. Rev. 102 (2002) 2187–2210.
[5] J. Inanaga, H. Furuno, T. Hayano, Chem. Rev. 102 (2002) 2211–2226.
[6] D.M. Ciurtin, M.D. Smith, H.C. zur Loye, Chem. Commun. (2002) 74–75.
[7] X.M. Zhang, M.L. Tong, X.M. Chen, Angew. Chem. Int. Ed. 41 (2002) 1029–1031.
[8] J.Y. Lu, Coord. Chem. Rev. 246 (2003) 327–347.
[9] M.B. Zhang, J. Zhang, S.T. Zheng, G.Y. Yang, Angew. Chem. Int. Ed. 44 (2005) 1385–1388.
[10] W.G. Lu, C.Y. Su, T.B. Lu, L. Jiang, J. Am. Chem. Soc. 128 (2006) 34–35.
[11] R.Q. Zou, H. Sakurai, Q. Xu, Angew. Chem. Int. Ed. 45 (2006) 2542–2546.
[12] M.H. Alkordi, Y.L. Liu, R.W. Larsen, J.F. Eubank, M. Eddaoudi, J. Am. Chem. Soc. 130 (2008) 12639–12641.
[13] G.G. Gao, L. Xu, W.J. Wang, X.S. Qu, H. Liu, Y.Y. Yang, Inorg. Chem. 47 (2008) 2325–2333.
[14] R.Q. Zhong, R.Q. Zou, M. Du, N. Takeichi, Q. Xu, Cryst. Eng. Comm. 10 (2008) 1175–1179.
[15] M.H. Alkordi, J.A. Brant, L. Wojtas, V.C. Kravtsov, A.J. Cairns, M. Eddaoudi, J. Am. Chem. Soc. 131 (2009) 17753–17755.
[16] Z.G. Gu, Y.P. Cai, H.C. Fang, Z.Y. Zhou, P.K. Thallapally, J.A. Tian, J. Liu, G.J. Exarhos, Chem. Commun. 46 (2010) 5373–5375.
[17] T.K. Maji, G. Mostafa, H.C. Chang, S. Kitagawa, Chem. Commun. (2005) 2436–2438.
[18] Z.Y. Li, J.W. Dai, H.H. Qiu, S.T. Yue, Y.L. Liu, Inorg. Chem. Commun. 13 (2010) 452–455.

[19] S.A. Wang, L.R. Zhang, G.H. Li, Q.S. Huo, Y.L. Liu, Cryst. Eng. Comm. 10 (2008) 1662–1666.
[20] F.W. Zhang, Z.F. Li, T.Z. Ge, H.C. Yao, G. Li, H.J. Lu, Y.Y. Zhu, Inorg. Chem. 49 (2010) 3776–3788.
[21] X. Feng, B. Liu, L.Y. Wang, J.S. Zhao, J.G. Wang, N.S. Weng, X.G. Shi, Dalton Trans. 39 (2010) 8038–8049.
[22] W.Y. Wang, X.L. Niu, Y.C. Gao, Y.Y. Zhu, G. Li, H.J. Lu, M.S. Tang, Cryst. Growth Des. 10 (2010) 4050–4059.
[23] S.R. Zheng, S.L. Cai, M. Pan, T.T. Xiao, J. Fan, W.G. Zhang, Cryst. Eng. Comm. 13 (2010) 883–888.
[24] X. Li, B.L. Wu, C.Y. Niu, Y.Y. Niu, H.Y. Zhang, Cryst. Growth Des. 9 (2009) 3423–3431.
[25] X.M. Jing, H. Meng, G.H. Li, Y. Yu, Q.S. Huo, M. Eddaoudi, Y.L. Liu, Cryst. Growth Des. 10 (2010) 3489–3495.
[26] X.M. Jing, L.R. Zhang, T.L. Ma, G.H. Li, Y. Yu, Q.S. Huo, M. Eddaoudi, Y.L. Liu, Cryst. Growth Des. 10 (2010) 492–494.
[27] X. Li, B.L. Wu, R.Y. Wang, H.Y. Zhang, C.Y. Niu, Y.Y. Niu, H.W. Hou, Inorg. Chem. 49 (2010) 2600–2613.
[28] G.J. Liu, G.W. Zhao, L. Li, H.T. Gao, Acta Crystallogr. E67 (2011) O488.
[29] W. Liu, G. Zhang, X. Li, B.L. Wu, H.Y. Zhang, Acta Crystallogr. E65 (2009) m938.
[30] G.M. Sheldrick, SADABS, Program for Empirical Absorption Correction of Area Detector Data, University of Göttingen, Göttingen, Germany, 1996.
[31] G.M. Sheldrick, SHELX 97, Program for Crystal Structure Solution and Refinement, University of Göttingen, Göttingen, Germany, 1997.
[32] P.H. Benjamin, C. Radu, Cryst. Growth Des. 9 (2009) 2539–2555.
[33] A. Fratini, G. Richards, E. Larder, S.S. Wavey, Neodymium, Inorg. Chem. 47 (2008) 1030–1036.
[34] A. Fratini, S. Swavey, Inorg. Chem. Commun. 10 (2007) 636–638.
[35] Z.H. Zhang, T.A. Okamura, Y. Hasegawa, H. Kawaguchi, L.Y. Kong, W.Y. Sun, N. Ueyama, Inorg. Chem. 44 (2005) 6219–6227.
[36] X. Feng, B. Liu, L.Y. Wang, J.S. Zhao, N.S. Weng, X.G. Shi, Dalton Trans. 39 (2010) 8038–8049.
[37] S. Quici, M. Cavazzini, G. Marzanni, G. Accorsi, N. Armaroli, B. Ventura, F. Barigellett, Inorg. Chem. 44 (2005) 529–537.
[38] F. Luo, Y. Che, J. Zheng, Cryst. Growth Des. 8 (2008) 2006–2010.
[39] M.S. Liu, Q.Y. Yu, Y.P. Cai, C.Y. Su, X.M. Lin, X.X. Zhou, J.W. Cai, Cryst. Growth Des. 8 (2008) 4083–4091.
[40] X. Yang, R.A. Jones, W.K. Wong, Chem. Commun. (2008) 3266–3268.
[41] X.W. Zhao, Q.F. Wu, H.J. Liu, M. Shao, H.P. Xiao, M.X. Li, Cryst. Eng. Comm. (2010) 1139–1146.